



**HAL**  
open science

## Directing peptide crystallization through curvature control of nanotubes ‡

Frédéric Gobeaux, Christophe Tarabout, Nicolas Fay, Cristelle Mériadec,  
Melinda Ligeti, David-Alexandre Buisson, Jean-Christophe Cintrat, Franck  
Artzner, Maité Paternostre

### ► To cite this version:

Frédéric Gobeaux, Christophe Tarabout, Nicolas Fay, Cristelle Mériadec, Melinda Ligeti, et al.. Directing peptide crystallization through curvature control of nanotubes ‡. *Journal of Peptide Science*, 2014, 20 (7), pp.508-516. 10.1002/psc.2647 . cea-01201911

**HAL Id: cea-01201911**

**<https://cea.hal.science/cea-01201911>**

Submitted on 18 Sep 2015

**HAL** is a multi-disciplinary open access archive for the deposit and dissemination of scientific research documents, whether they are published or not. The documents may come from teaching and research institutions in France or abroad, or from public or private research centers.

L'archive ouverte pluridisciplinaire **HAL**, est destinée au dépôt et à la diffusion de documents scientifiques de niveau recherche, publiés ou non, émanant des établissements d'enseignement et de recherche français ou étrangers, des laboratoires publics ou privés.



# Directing peptide crystallization through curvature control of nanotubes<sup>‡</sup>

Frédéric Gobeaux,<sup>a,b,c</sup> Christophe Tarabout,<sup>b</sup> Nicolas Fay,<sup>a,b</sup>  
Cristelle Meriadec,<sup>b</sup> Melinda Ligeti,<sup>d</sup> David-Alexandre Buisson,<sup>d</sup>  
Jean-Christophe Cintrat,<sup>d</sup> Franck Artzner<sup>b,\*\*</sup> and Maité Paternostre<sup>a,\*</sup>

In the absence of efficient crystallization methods, the molecular structures of fibrous assemblies have so far remained rather elusive. In this paper, we present a rational method to crystallize the lanreotide octapeptide by modification of a residue involved in a close contact.

Indeed, we show that it is possible to modify the curvature of the lanreotide nanotubes and hence their diameter. This fine tuning leads to crystallization because the radius of curvature of the initially bidimensional peptide wall can be increased up to a point where the wall is essentially flat and a crystal is allowed to grow along a third dimension. By comparing X-ray diffraction data and Fourier transform Raman spectra, we show that the nanotubes and the crystals share similar cell parameters and molecular conformations, proving that there is indeed a structural continuum between these two morphologies. These results illustrate a novel approach to crystallization and represent the first step towards the acquisition of an Å-resolution structure of the lanreotide nanotubes  $\beta$ -sheet assembly. Copyright © 2014 European Peptide Society and John Wiley & Sons, Ltd.

Additional supporting information may be found in the online version of this article at the publisher's web site.

**Keywords:** self-assembly; crystallization; nanotubes; size-control; diameter-control;  $\beta$ -sheet

## Introduction

Because of their implication in many human neurodegenerative disorders such as Alzheimer's, Parkinson's, Huntington's or prion diseases, amyloid fibres have spurred numerous studies [1]. Deciphering their structure and assembly mechanisms has been a challenge to understand and hopefully prevent these diseases. This comprehension is unfortunately intrinsically limited because of their fibrillar nature. Indeed, fibres are generally one-dimensional and non-crystalline objects, from which it is difficult to get structural information with traditional techniques such as X-ray diffraction and high-resolution nuclear magnetic resonance (NMR) spectroscopy. Fibre diffraction brings much less information than that of a tridimensional single crystal and relies on an often delicate processing of the fibres to align them, either by shearing or by application of an external electro-magnetic field. Moreover, the study of the pathological amyloid structures is also impeded because their assembly is under kinetic control, which often results in irreversibility and in a high degree of polymorphism [2–5]. In fact, most of these issues are rather general to fibrillar bioassemblies and still today much work is devoted to determine or improve the resolution of the structure of crucial structural proteins such as collagen [6], actin [7], microtubules [8,9] and intermediary filaments [10–12]. Likewise, the structures of elongated and rod-like viruses have also been widely investigated [13–17].

In the specific case of amyloid fibres, strategies using shorter peptides have been set up to obtain high-resolution ( $\sim 1$  Å) structures of the  $\beta$ -sheet amyloid fibres. A method that proved its worth consists in selecting short segments of fibrils-forming proteins such as synuclein [18], Sup35 [19,20], insulin [21], amyloid- $\beta$  [22] or  $\alpha$ B-crystallin [23] and to crystallize them. Makabe

*et al.* [24] used the 'link-and-cap' strategy: they covalently linked a defined number of peptide units to prevent sample heterogeneity and capped the extremities of the units to prevent further lateral aggregation or lamination. These approaches allow determining the atomic structure of individual elements such as elementary  $\beta$ -strand building blocks and their further assembly into steric zippers, but the full picture of the fibrils remains elusive, especially because of their widespread polymorphism. More recently, Fitzpatrick *et al.* reported the atomic-resolution (0.5 Å) structures of three polymorphic cross- $\beta$  amyloid fibrils formed by an 11-residue peptide

\* Correspondence to: Maité Paternostre, iBiTec-S, SB<sup>2</sup>SM, UMR 8221, CEA/CNRS, CEA-Saclay, 91191 Gif-sur-Yvette, France. E-mail: maité.paternostre@cea.fr

\*\* Correspondence to: Franck Artzner, Institut de Physique de Rennes, UMR 6251 CNRS/Université Rennes 1, Campus Beaulieu, 35042 Rennes Cedex, France. E-mail: franck.artzner@univ-rennes1.fr

<sup>‡</sup> This article is published in *Journal of Peptide Science* as part of the Special Issue devoted to contributions presented at the 1st International Conference on Peptide Materials for Biomedicine and Nanotechnology, Sorrento, October 28–31, 2013, edited by Professor Giancarlo Morelli, Professor Claudio Toniolo and Professor Mariano Venanzi.

a iBiTec-S, SB<sup>2</sup>SM, UMR 8221, CEA/CNRS, CEA-Saclay, 91191 Gif-sur-Yvette, France

b Institut de Physique de Rennes, UMR 6251 CNRS/Université Rennes 1, Campus Beaulieu, 35042, Rennes Cedex, France

c Laboratoire Interdisciplinaire sur l'Organisation Nanométrique et Supramoléculaire (LIONS), IRAMIS, NIMBE, UMR 3299 CEA/CNRS CEA-Saclay, 91191 Gif-sur-Yvette Cedex, France

d iBiTec-S, SCBM, CEA-Saclay, 91191 Gif-sur-Yvette, France

using a combination of NMR, cryo-EM, X-ray fibre diffraction, STEM and AFM [25]. Besides, this work illustrates that resolving a structure remains a long-term endeavour and emphasizes the necessity to combine several biophysical techniques to reach this goal.

In the present paper, we expose a crystallization approach that consists in a minor chemical modification carried out on a single lateral side chain that does not modify the peptide packing but allows the crystallization of the system. This approach has been implemented on the lanreotide. Lanreotide is a synthetic octapeptide whose full sequence is detailed in the Material and Methods section and whose extended formula is displayed in Figure 1A. Its most specific chemical features are (i) a disulfide bond between two cysteine residues that cyclizes the molecule and stabilizes a hairpin configuration; (ii) two cationic charges; (iii) three aromatic residues segregated on one branch of the hairpin; (iv) two unnatural amino acids (D-naphthylalanine and D-tryptophan). These features confer to the lanreotide peptide its remarkable self-assembly properties in pure water. It has indeed been shown that when the lanreotide-acetate salt is solubilized above a critical assembly concentration of 20 mM, it spontaneously self-assembles into nanotubes with a strictly constant diameter of 24.4 nm [26,27]. The walls of these nanotubes are formed by a two-dimensional crystalline bilayer. The stacking of the peptides in these two layers is different (Figure 1A and B), but both are structured in one direction by a H-bond network forming an antiparallel  $\beta$ -sheet and in the other by close contacts between lateral chains, either in the  $\beta$ -turn or at the N-terminus of the molecule. Finally, these nanotubes are in a dynamic equilibrium with monomers and

dimers [28], and they form a hexagonal columnar liquid crystalline phase [26,27].

Several chemical modifications on the lanreotide amino acid sequence and their consequences on the supramolecular assembly have already been reported [29,30]. For example, opening the lanreotide cyclic backbone either by replacing the cysteine by alanines or by reducing the disulfide bridge with  $\beta$ -mercaptoethanol leads to the formation of curved lamellae. Inverting the chirality of the lysine residues from L to D configuration leads to formation of fibres, while placing a D-phenylalanine instead of the D-naphthylalanine or of the L-tyrosine leads to the formation of micelles. In another case, the deletion of the D-tryptophan residue totally prevents self-assembly. These modifications clearly underline the specificity of the amino acids sequence leading to the assembly of well-defined monodisperse nanotubes.

More interestingly, it was also demonstrated that the slight modification of the side chain of a single residue involved in a steric close contact allowed for the fine tuning of the diameter of the nanotubes [31]. Indeed, replacing the D-tryptophan in the fourth position by aromatic residues of different size allows creating a library of peptides forming nanotubes of diameters ranging from 10 to 36 nm. This was explained by a simple geometrical model (Figure 1C and D) showing that the nanotubes diameter is proportional to the size of the aromatic side chains because these latter are involved in a close contact localized in the inner layer of the nanotube wall (Figure 1B).

Additionally to such chemical modifications, counter-ions can also be used to induce morphological changes in supramolecular

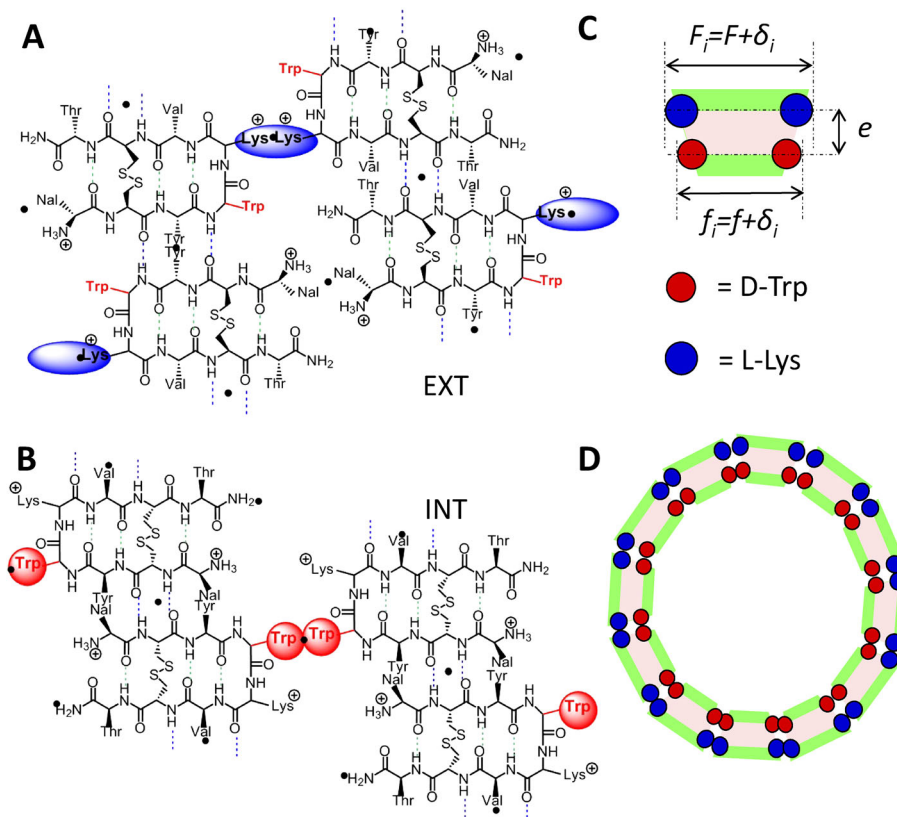


**Figure 1.** Molecular packing of the lanreotide peptide in the nanotube walls and corresponding geometrical model based on the simplified projection of the unit cell. The wall is made of two layers: (A) Outer layer of the nanotube wall and (B) inner layer of the nanotube wall. (C) Schematic top view of a group of two lanreotide dimers (minimal building block of the wall, which defines its thickness). The hydrophobic surfaces are in green, aromatic ones in red and aliphatic ones in blue. (D) Top view of a lanreotide nanotube section highlighting the close contacts between aromatic residues (in red) in the inner layer and between the aliphatic residues (in blue) in the outer layer.

assemblies [32–36]. In the particular case of lanreotide nanotubes, we have previously shown that both diameter and number of walls can be modulated by using counter-ions of respectively different sizes [37] and valences [38].

The observation of the molecular packing of the lanreotide monomers in the nanotubes suggests that close contacts between aliphatic residues of adjacent dimers may also exist. In particular, the lysine side chain could be involved in such close contacts, this time in the outer layer of the peptide wall (Figure 1A), contrary to the aforementioned close contacts observed between aromatic residues. We thus expect that a size modification on this location would also contribute to change the nanotube diameter, but that this effect would be the opposite. Indeed, as the geometric model previously devised [31] suggests it (Figure 1C and D), the curvature of the nanotubes should *increase* when the local steric hindrance *decreases*. In the present work, we therefore probed the influence of the aliphatic side chain length of the amino acid residue in position 5. We used transmission electron microscopy (TEM), small angle X-ray scattering (SAXS), Fourier transform Raman and Fourier transform infrared (FTIR) spectroscopies to characterize the structures of the corresponding peptide assemblies.

## Results

### Influence of the Lysine Side Chain Length



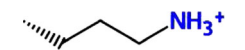
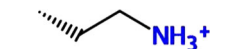
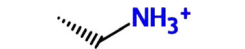
The influence of the aliphatic side chain of the amino acid residue in position 5 was probed by synthesizing lanreotide derivatives with L-dimethyl-lysine, L-ornithine, L-1,4-diamino-butyric acid or L-1,3-diamino propionic acid, instead of the L-lysine (Materials and Methods section). We will refer to the corresponding derived peptides respectively as derivative 1, 2, 3 and 4 (Table 1).

These peptides were solubilized at room temperature in pure water at concentrations above 20 mM. The derivatives 1, 2 and 3 form translucent gels similar to the one obtained with lanreotide. A negatively stained transmission electron micrograph of a derivative 3 sample – but representative of these three derivatives – is

displayed in Figure 2A. It shows that the gels are formed of self-assembled peptide nanotubes. This nanotube structure is confirmed by the typical oscillations of the SAXS patterns displayed in Figure 2C (Traces L and 1–3). Indeed, these oscillations can be fitted by normalized Bessel functions of zeroth order  $[J_0(q*r_0)/q]^2$  that are the theoretical form factors of infinite hollow cylinders [39]. The nanotubes radius  $r_0$  can thus be extracted from this mathematical model, while the high number of oscillations (more than ten) gives an indication of the very low polydispersity. We give the corresponding diameters for each peptide in Table 1. Moreover, the three reflections between 0.35 and 0.37 Å<sup>-1</sup> corresponding to repetitive distances between 17 and 18 Å can be assigned to a  $\beta$ -sheet network resulting from an alternated stacking of antiparallel peptides (Figure 1A and Valéry *et al.* [26]). The FTIR spectra in the amide I region (Figure 2D) support this interpretation. Indeed, the bands at 1694 and 1614 cm<sup>-1</sup> are the characteristic features of antiparallel  $\beta$ -sheets. Moreover, all the spectra display bands attributed to a turn (1664 cm<sup>-1</sup>) and to a random conformation at 1640 cm<sup>-1</sup>. All these features were previously observed and interpreted in details for the lanreotide peptide nanotubes [26,27].

In the case of the derivative 4, some polymorphism is observed. If the peptide powder is solubilized at room temperature, a milky liquid is instantaneously obtained, whereas if solubilization occurs at 70 °C, a transparent gel forms after cooling down to room temperature. SAXS data (Figure 2C, trace 4) demonstrate that this gel is made of 31.4-nm wide nanotubes. Depending on the TEM sample preparation, other morphologies such as filaments or some sparse microcrystals may be observed (Figure S1). TEM observations of the milky liquid obtained at room temperature reveal that it is actually a suspension of micron-size needle-shaped crystals that scatter light (Figure 2B) and are dense enough to the electrons to be imaged without staining (Figure S1A). The X-ray powder diffraction pattern of such a sample (Figure 2D, trace 4\*) confirms the crystalline nature of these objects. The diffraction peaks were indexed in a monoclinic cell. The full indexing of the peaks is reported in Table 2 and the corresponding cell parameters in Table 3. These parameters are very close to those of the 2D cells

**Table 1.** Nomenclature of the peptide studied in the paper and diameters of the corresponding nanotubes as measured by analysis of SAXS patterns

| Name of the peptide | Residue in position 4        | Side chain of the residue in position 4   | Length of the aliphatic chain <sup>a</sup> (Å) | Nanotube diameter (nm) |
|---------------------|------------------------------|---|--|------------------------|
| Lanreotide (L)      | L-lysine                     |  | 8.3  | 24.4                   |
| Derivative 1        | L-dimethyl-lysine            |  | 8.4  | 25                     |
| Derivative 2        | L-ornithine                  |  | 7.1  | 25.7                   |
| Derivative 3        | L-1,4-diamino-butyric acid   |  | 5.8  | 27.3                   |
| Derivative 4        | L-1,3-diamino propionic acid |  | 4.6  | 31.4/crystals          |

<sup>a</sup>The length of the extended aliphatic chain was determined using ChemDraw.

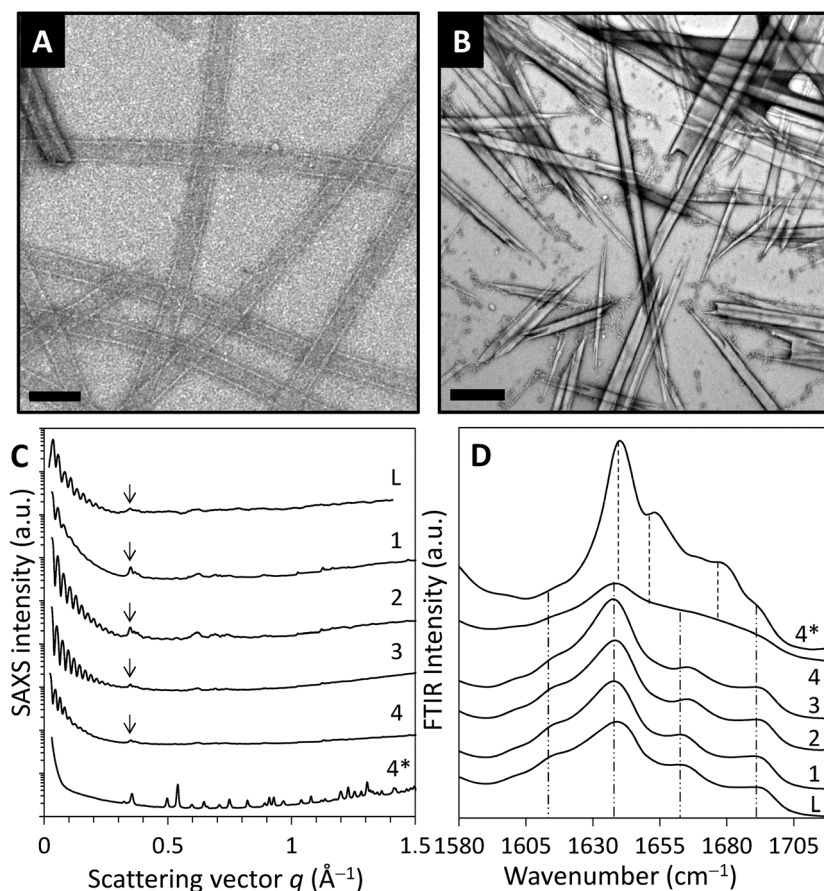


**Figure 2.** Influence of the lysine side chain length on the peptide assembly. (A) Negatively stained electron micrographs of derivative 3. Scalebar = 100 nm. (B) TEM micrograph of derivative 4 microcrystals in water. Scalebar = 1  $\mu\text{m}$ . (C) SAXS profiles of the lanreotide (trace L) and of the four lysine-modified derivatives. For the derivative 4, profiles corresponding to the both nanotubes (4) and crystals (4\*) forms are shown. The grey arrows points out the reflection at  $0.35 \text{ \AA}^{-1}$  indicative of an antiparallel  $\beta$ -sheet network (refer to main text for details). (D) ATR-FTIR spectra of lanreotide and four derivatives.

of the nanotubes [26]. It is thus very likely that 2D peptide walls are piling up to form 3D crystals, albeit with a slight deformation. As the correlation length estimated from the full width at half-maximum of the diffraction peaks ( $\zeta = 2\pi/\Delta q$ ) is only 56 nm long – which is rather small compared to the dimensions measured on the micrographs – we cannot discard the possibility that the crystals are twinned. FTIR spectrum of the centrifuged pellet appears slightly more defined than that of previous one. Although characteristic vibrations due to antiparallel  $\beta$ -sheet are present, new vibrations are detected at  $1653$  and  $1678 \text{ cm}^{-1}$ . On the contrary, the comparison of the FT-Raman spectra of the lanreotide nanotubes and of the derivative 4 microcrystals suggests that the conformation of the aromatic residues is similar in both structures (Figure 3).

Indeed, Raman spectroscopy is commonly used to provide information on structural features of peptide and proteins as secondary structures and markers of side chain environments [40–42]. Here, the Raman spectra provide fingerprints of the aromatic side chains environment of lanreotide within each assembly. The full spectra of the lanreotide nanotubes (top spectrum) and of the centrifuged microcrystals of derivative 4 (bottom spectrum) are presented in Figure 3. The main peaks can be assigned to the aromatic residues (D-tryptophan, L-tyrosine and D-naphthylalanine). Because of the presence of these three aromatic residues, overlaps may exist, and therefore we do not give detailed assignments of the full spectra. Some other peaks are due

to the disulfide bridge ( $495\text{--}525 \text{ cm}^{-1}$ ) and to the  $\beta$ -sheet conformation ( $1640\text{--}1700 \text{ cm}^{-1}$ ). Most of these peaks are common in the two spectra, indicating that the side chains conformations are similar in both the nanotubular and the microcrystalline forms. In particular, the very intense peaks assigned to tryptophane side chains (W18:  $768.8 \text{ cm}^{-1}$ , W16:  $1013.7 \text{ cm}^{-1}$ , W15:  $1085.06 \text{ cm}^{-1}$ , W7:  $1382.08 \text{ cm}^{-1}$ , W6:  $1438.01 \text{ cm}^{-1}$ ) or tyrosine ( $631.81$  and  $1613.53 \text{ cm}^{-1}$ ) are indeed found in the same position in both spectra indicating a very close environment of tryptophan in both nanotubes and crystals. Slight differences can be observed between the two spectra (Figure 3, pointed out with #), mostly in wavenumbers ranges assignable to tyrosine ( $820\text{--}850$  and  $1210\text{--}1180 \text{ cm}^{-1}$ ). However, these differences occur with peaks of low intensity whose signal can be mingled with noise, so these differences are probably marginal.

## Discussion

In the present work, we show that the decrease of the aliphatic chain length of the L-lysine (i.e. the amino acid in the position 5 of the lanreotide sequence) leads to the formation of self-assembled peptide nanotubes of increasing diameter from  $24.4$  to  $31.4 \text{ nm}$ . The wall of the lanreotide nanotube is made from a bilayer, both layers being formed by the lateral association of antiparallel  $\beta$ -sheet protofilaments. The close contacts between the protofilaments are

**Table 2.** Peak indexation of the diffraction pattern exhibited in Figure 2C (trace 4<sup>a</sup>)

| Miller indices <i>hkl</i> | $q_{th}$ | $q_{exp}$     | Error              |
|---------------------------|----------|---------------|--------------------|
| 1 0 0                     | 0.3235   | 0.3234        | 1.10 <sup>-4</sup> |
| 1 0 -1                    | 0.3554   | 0.3545        | 9.10 <sup>-4</sup> |
| 1 1 0                     | 0.4979   | 0.4972        | 7.10 <sup>-4</sup> |
| 1 0 1                     | 0.5370   | 0.5399        | 3.10 <sup>-3</sup> |
| -2 0 1                    | 0.5994   | 0.5972        | 2.10 <sup>-3</sup> |
| 2 0 0                     | 0.6470   | 0.6460        | 1.10 <sup>-3</sup> |
| 1 1 1                     | 0.6570   | 0.6578        | 8.10 <sup>-4</sup> |
| -2 1 1                    | 0.7089   | 0.7083        | 6.10 <sup>-4</sup> |
| 2 -1 0                    | 0.7496   | 0.7485        | 1.10 <sup>-3</sup> |
| 0 2 1                     | 0.8220   | 0.8215        | 6.10 <sup>-4</sup> |
| 1 1 2                     | 0.9059   | 0.8914        | 1.10 <sup>-2</sup> |
| 2 1 1                     | 0.9052   | 0.9099        | 8.10 <sup>-4</sup> |
| 1 2 1                     | 0.9281   | 0.9279        | 2.10 <sup>-4</sup> |
| 3 0 0                     | 0.9705   | 0.9683        | 2.10 <sup>-3</sup> |
| 3 1 0                     | 1.0417   | 1.0395        | 2.10 <sup>-3</sup> |
| 2 0 2                     | 1.0740   | 1.0786        | 5.10 <sup>-3</sup> |
| 2 2 1                     | 1.1209   | 1.1207        | 2.10 <sup>-4</sup> |
| 0 3 0                     | 1.1355   | 1.1355        | 3.10 <sup>-5</sup> |
| 3 1 1                     | 1.1962   | 1.2000        | 4.10 <sup>-3</sup> |
| 0 -2 3                    | 1.2236   | 1.2290        | 5.10 <sup>-3</sup> |
| 1 3 1                     | 1.2561   | 1.2544        | 2.10 <sup>-3</sup> |
| 0 0 4                     | 1.2818   | 1.2816        | 2.10 <sup>-4</sup> |
| 2 3 0                     | 1.3069   | 1.3060        | 9.10 <sup>-4</sup> |
| 2 2 2                     | 1.3140   | 1.3182        | 4.10 <sup>-3</sup> |
| 3 1 -4                    | 1.3252   | 1.3278        | 3.10 <sup>-3</sup> |
| 2 3 -2                    | 1.3397   | 1.3467        | 7.10 <sup>-3</sup> |
| 1 2 3                     | 1.3583   | 1.3649        | 7.10 <sup>-3</sup> |
| 3 1 2                     | 1.4078   | 1.4135        | 6.10 <sup>-3</sup> |
| -2 3 3                    | 1.4650   | 1.4655        | 9.10 <sup>-4</sup> |
| 0 3 3                     | 1.4878   | 1.4829        | 5.10 <sup>-4</sup> |
| 4 1 1                     | 1.4981   | 1.4973        | 5.10 <sup>-3</sup> |
| 0 4 0                     | 1.5140   | 1.5119        | 9.10 <sup>-4</sup> |
| 5 0 -3                    | 1.5249   | 1.5314        | 2.10 <sup>-3</sup> |
| 1 4 -1                    | 1.5530   | 1.5544        | 6.10 <sup>-3</sup> |
| 5 0 0                     | 1.5552   | 1.5544        | 1.10 <sup>-3</sup> |
| 4 2 1                     | 1.6353   | 1.6352        | 1.10 <sup>-4</sup> |
| 3 1 3                     | 1.6548   | 1.6519        | 3.10 <sup>-3</sup> |
| 4 1 2                     | 1.6960   | 1.6983        | 2.10 <sup>-3</sup> |
|                           |          | Average error | 3.10 <sup>-3</sup> |
|                           |          | Maximum error | 1.10 <sup>-2</sup> |
| Not observed              | $q_{th}$ |               |                    |
| 0 0 1                     | 0.3205   |               |                    |
| 0 1 0                     | 0.3785   |               |                    |
| 0 0 2                     | 0.6409   |               |                    |
| 0 2 0                     | 0.7570   |               |                    |
| 4 0 0                     | 1.2940   |               |                    |
| 0 0 5                     | 1.6023   |               |                    |

provided by the D-tryptophan for the inner layer and by L-lysine for the outer one [31]. In a previous work, we have shown that increasing the steric hindrance of the amino acid providing the close contact between protofilaments in the inner layer, that is, the D-tryptophan, increases the nanotube diameter from 24.4 to 31.4 nm. This fine diameter tuning was explained and predicted by a simple geometrical model [31]. By using the same model, the increase of the diameter by the decrease of the steric hindrance of the close contacts on the outer layer, that is, the amino acid in position 5, is also predicted, as illustrated in Figure 4A. The equation 1 is deduced from the model (refer to Supporting Information):

$$\delta_i = (f - F) - 2F \frac{e}{D_i} \quad (1)$$

$F$  and  $f$  are the distances between two close contacts in the outer and inner layers respectively and  $e$  the thickness of the bilayer that constitutes the nanotube wall. These parameters are illustrated in Figure 1C. For the present experiments,  $\delta_i$  has been estimated using Chemdraw to measure the length of the different lateral chains introduced in position 5 (Table 1).

On Figure 4B (triangles), the plot of  $\delta_i$  as a function of the inverse of the nanotubes diameter exhibits a linear evolution with a positive slope as expected from Eqn 1. However, the structural parameters  $f$ ,  $F$  and  $e$  (extracted from the origin and slope of the straight line) are different from the values known from the structural model [31]. This misfit can be ascribed to the discrepancy between our values of  $\delta_i$  measured for fully extended aliphatic chains and the real values  $\delta_i$  for flexible chains. Nevertheless, these experiments extend the validity of the geometrical model to the close contacts present on the outer layer of the nanotubes walls.

A molecular steric modification of the order of the ångström (length of the lysine side chain) therefore leads to modifications of the diameter dimension of the order of the nanometre. Here, one must point out that this change of diameter comes with an accommodation of the number of molecules in the perimeter so that the environment of the close contacts that are untouched by the chemical modification does not change.

In addition to the present data, we have plotted on Figure 4B most of the data from Tarabout *et al.* [31] (diamonds) and Gobeaux *et al.* [37] (circles). The ordinate reads the 'normalized' hindrance of the modifications, whether it is a chemical modification of the aromatic residue in position 4 (open diamonds), on the aliphatic residue on position 5 (triangles) or a change of counterions (circles). We have chosen the lanreotide-acetate condition as a reference ( $\delta_i = 0$ ,  $D = 24.4$  nm,  $1/D = 0.041$  nm<sup>-1</sup>).

Comparing the slopes of the plots of these three sets of data corresponding to the three possible 'triggers' may give us insight on the strength of each lever arm to control the nanotubes diameter. In this respect, the most efficient 'trigger' appears to be the aromatic residue in the position 4, while the respective effects of changing the counter-ions or modifying the length of

**Table 3.** Unit cell parameters of the nanotubes walls and of the crystals

|   | $a$ (Å) | $b$ (Å) | $c$ (Å) | $\alpha$ (°) | $\beta$ (°) | $\gamma$ (°) | $V$ (Å <sup>3</sup> ) |
|---|---------|---------|---------|--------------|-------------|--------------|-----------------------|
| Lanreotide NT (2D crystal) <sup>a</sup> | 20.7    | —       | 20.8    | —            | 119         | —            | 7000                  |
| Derivative 4 (crystals)                 | 21.1    | 16.6    | 21.3    | 90           | 113         | 90           | 6870                  |

<sup>a</sup>Cell parameters taken from Valéry *et al.* [26].

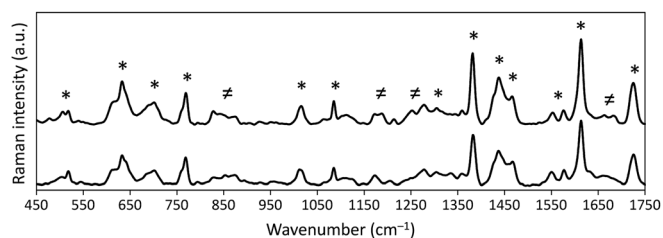


**Figure 3.** FT-Raman comparison of nanotubular and microcrystalline forms. (A) FT-Raman spectra of 10%w/w lanreotide nanotubes gel (top graph) and of centrifuged microcrystals of derivative 4 (bottom graph). The symbols '\*' and '#' respectively indicate similar and differing peaks.

the aliphatic side chain on position 5 are of the same order of magnitude. Indeed, when a 1-Å modification is introduced on the position 4, the nanotubes diameter changes on average of 10.2 nm, whereas a 1-Å modification is introduced on the position 5, the diameter only changes of 1.7 nm. The lesser strength of the aliphatic lever arm may be explained by the fact that the molecular packing is slightly less dense in the outer layer than in the inner layer. Additionally, the close contacts between aliphatic residues may be less rigid than between aromatic ones.

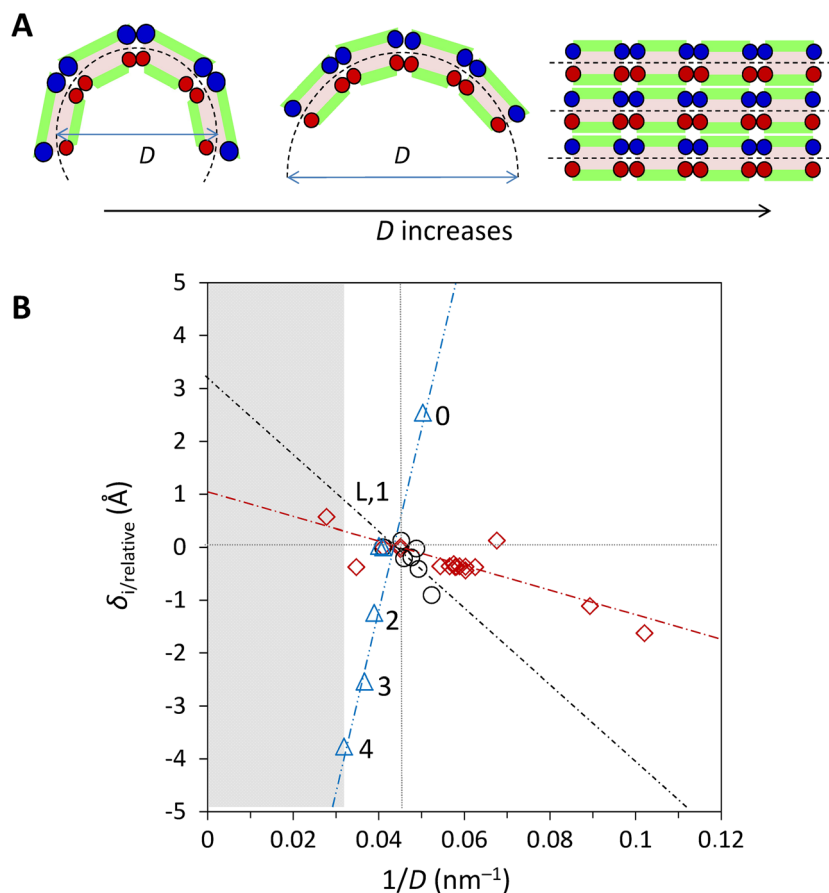


**Figure 4.** (A) Geometrical illustration of the formation of crystals as a limit-case when the radius of curvature tends to infinity because the steric hindrance (symbolized by blue beads) of the close contacts in the outer layer is getting smaller. (B) Plots of the characteristic dimensions of the hindrance  $\delta_{i/relative}$  for each 'trigger' as a function of the inverse of the measured diameters in accordance to the geometric model. The  $\delta_i$  have been scaled so that  $\delta=0$  for the lanreotide-acetate condition (located at the centre of the cross-hair). Black open circles corresponds to the counter-ions exchanges on the lanreotide; the red diamonds ( $\diamond$ ) to the modifications of the aromatic residue on position 4 and the blue triangles ( $\Delta$ ) to the modifications on the aliphatic side chain on position 5. The lines are guides to the eye, and the grey area indicates the region where we experimentally observe crystals. This diagram colligates data from this study and from references [31,37]. NB: The datapoint tagged 0 corresponds to a lanreotide derivative whose lysine side chain has been acetylated. This derivative self-assembles into nanotubes of 19.9-nm diameter. The complete characterization of this peptide has been previously published in Gobeaux *et al.* [37].

Figure 4B also illustrates that the three triggers do not have the same range of application. Modifications of the aromatic residue on position 4 allows for a wide range of diameters from 10 to 36 nm, whereas the counter-ions exchange provides a finer tuning in the 19–26-nm range. Modifications of the aliphatic residue on the position 5 'fill the gap' in the 26–32-nm range. Moreover, the 'counter-ion trigger' can basically be used on any molecule. One can thus envision reaching an even finer tuning of the nanotubes diameter by using the three triggers on a single molecule.

Finally, at the  $y$ -intercept the model gives theoretical values of  $\delta_i$  for which the curvature of the nanotubes becomes flat, because the diameter  $D$  tends to infinity. According to the experimental results, it seems that the span of the nanotube diameter range is upper bounded by a value of the order of 30–35 nm. Indeed, above this boundary, we rather observe crystals than nanotubes. This 'crystallization zone' is coloured in light grey in Figure 4B.

As a matter of fact, our study does suggest that there is a structural continuum between the nanotubes and the crystals and that the latter are a borderline case when the radius of curvature becomes very large. Indeed, X-ray diffraction reveals that both 2D and 3D crystals are made of monoclinic cells (Table 3). The parameters  $a$  and  $c$  correspond to the parameters of a bilayer cell

while the parameter  $b = 16.6 \text{ \AA}$ , which is slightly lower than the  $18 \text{ \AA}$  in the lanreotide nanotube cell, represents the thickness of a dimer. Four peptides can fit in the volume  $V = 6870 \text{ \AA}^3$ , which corresponds to two dimers attached by hydrogen bonds. The symmetry elements due to the monoclinic cell suggest that the dimers are exactly piled on top of each other along the third direction without any position inversion between the hydrophilic zones. This means that the elements constitutive of the outer layer in the nanotubes are directly superimposed on the elements constitutive of the inner layer in the nanotubes. As a consequence, there is a  $C_2$  symmetry axis along  $b$ , perpendicularly to the dimer thickness, oriented in the same direction as in the lanreotide nanotube layers. Additionally, the Raman spectra of the two forms exhibit very similar fingerprints (Figure 3). The differences observed in the ATR-FTIR spectra might simply be attributed to the high sensitivity of the technique to vibratory modes which obviously change when the curvature becomes flat.

Actually, we have found similar borderline cases with the other triggers, which will be reported elsewhere with complete structural details. Notwithstanding, the fact that all these crystallizing samples were part of series of samples with increasing nanotubes diameters emphasizes the generality of the approach. In some cases, depending on the followed kinetics path, both forms can be observed for the same physical–chemical condition.

A future perspective for this study is to obtain diffraction patterns of the crystals. We can consider using a microfocus beam [43], whose  $5\text{-}\mu\text{m}$  diameter may allow to shine X-ray on a single small crystal such as the ones exhibited in Figure 2B. We can also try to grow larger crystals by slowing down nucleation or by using our current crystals as seeds so as to perform more conventional diffraction experiment. Because peptides are small compared to proteins, a single crystal contains many more unit cells, and thus, we expect to reach a very high resolution, of the order of the ångström [19–22]. The detailed structure of the crystals with such a resolution would bring new and accurate informations on the interactions at the origin of the singular assembly of lanreotide and on the exact orientation of the aromatic residues in the layers. It would also give more insights on the origin of the interactions between the stacked bilayers that allow for the growth of the crystals along the  $b$ -axis.

## Conclusion

Overall, the present results along with those of previous work [31,37] show that lanreotide nanotubes formation is a robust process that can withstand to a certain extent chemical modifications of carefully chosen amino acids in the sequence (i.e. D-tryptophan on the fourth position and L-lysine on the fifth position) or exchange of the counter-ions. These approaches allow the tuning of the diameter of lanreotide nanotubes in the 10–36-nm range and lead to molecular crystallization. This may represent a first step towards the determination of the atomic structure of lanreotide nanotubes.

## Materials and Methods

### Materials

Lanreotide was obtained from Ipsen Pharma (Barcelona, Spain), and the derivatives were synthesized by solid-phase Fmoc/tBu chemistry. The peptide chain was first assembled and then cyclized on-resin. Cleavage and side chain deprotection were performed

simultaneously, followed by purification and counter-ion exchange [37,44]. Purity of the final products was checked by HPLC/MS (refer to the following text and Supporting Information). Peptide sequences are **lanreotide**: H-D-2-Nal<sup>1</sup>-cyclo(Cys<sup>2</sup>-Tyr<sup>3</sup>-D-Trp<sup>4</sup>-Lys<sup>5</sup>-Val<sup>6</sup>-Cys<sup>7</sup>)-Thr<sup>8</sup>-NH<sub>2</sub>; **derivative 1**: H-D-2-Nal<sup>1</sup>-cyclo(Cys<sup>2</sup>-Tyr<sup>3</sup>-D-Trp<sup>4</sup>-(Me)<sub>2</sub>Lys<sup>5</sup>-Val<sup>6</sup>-Cys<sup>7</sup>)-Thr<sup>8</sup>-NH<sub>2</sub>; **derivative 2**: H-D-2-Nal<sup>1</sup>-cyclo(Cys<sup>2</sup>-Tyr<sup>3</sup>-D-Trp<sup>4</sup>-Orn<sup>5</sup>-Val<sup>6</sup>-Cys<sup>7</sup>)-Thr<sup>8</sup>-NH<sub>2</sub>; **derivative 3**: H-D-2-Nal<sup>1</sup>-cyclo(Cys<sup>2</sup>-Tyr<sup>3</sup>-D-Trp<sup>4</sup>-Dab<sup>5</sup>-Val<sup>6</sup>-Cys<sup>7</sup>)-Thr<sup>8</sup>-NH<sub>2</sub>; **derivative 4**: H-D-2-Nal<sup>1</sup>-cyclo(Cys<sup>2</sup>-Tyr<sup>3</sup>-D-Trp<sup>4</sup>-Dap<sup>5</sup>-Val<sup>6</sup>-Cys<sup>7</sup>)-Thr<sup>8</sup>-NH<sub>2</sub>

### LC/MS Analysis and Purification

HPLC was performed using a Waters system (2525 binary gradient module, in-line degasser, 2767 sample manager, 2996 Photodiode Array Detector). The eluent was a gradient of A (99.9% water/0.1% HCOOH) and B (99.9% ACN/0.1% HCOOH). Either analytical or preparative X-bridge C18 columns were used. Retention times (rt) are given in Table S1.

The mass spectrometer was a Waters Micromass ZQ system with a ZQ2000 quadrupole analyser. The ionization was performed by electrospray, and the other parameters were as follows: source temperature  $120^\circ\text{C}$ , cone voltage 20V and continuous sample injection at 0.3 ml/min flow rate. Mass spectra were recorded in positive ion mode in the  $m/z$  100–2000 range and treated with the Mass Lynx 4.0 software. The experimental and calculated  $m/z$  are given in Table S1.

### NMR Analysis

The synthesized peptides were controlled by <sup>1</sup>HNMR on a Bruker Avance 400 Ultrashield. Spectra were recorded at room temperature at 400 MHz, and samples were dissolved in D<sub>2</sub>O at a concentration of approximately 5 mM. The D<sub>2</sub>O singlet signal was set up at 4.79 ppm. Chemical shifts are given in ppm and the coupling constants in Hz. The full characterizations are given in the Supporting Information text.

### Transmission Electron Microscopy

Transmission electron microscopy was performed on a Philips CM12 electron microscope operated at 80 kV. A drop of the solution at 3–5%w/w was put on a copper grid covered with a carbon film (Agar Scientific). After blotting off of the excess liquid, the material was stained with a 2% uranyl acetate solution.

### Small Angle X-ray Scattering

Small angle X-ray scattering experiments were either performed at the SWING beamline at the SOLEIL synchrotron (Saclay, France) or with a rotating anode laboratory set-up. X-ray patterns were detected and recorded via a CCD (chip charge-coupled device) camera detector. The samples were inserted in 1.3–1.6-mm round glass capillaries and centrifuged at the bottom. The scattering intensities as a function of the radial wave vector,  $q = 4\pi/\lambda \times \sin\theta$ , were determined by circular integration and tubes diameter were, when present, estimated by fitting the corresponding oscillations by normalized zeroth order Bessel functions  $J_0^2(qr_0)/q^2$  (Oster and Riley [39]). When the sample was crystalline, the powder diffraction Bragg peaks were simulated and indexed with McMaille [45].



### Fourier Transform Infrared Spectroscopy

Attenuated total reflectance Fourier transform infrared (ATR-FTIR) spectra were recorded at a  $2\text{-cm}^{-1}$  resolution with a Bruker IFS 66 spectrophotometer equipped with a  $45^\circ$  N ZnSe ATR attachment. The spectra obtained resulted from the average of 30 scans and were corrected for the linear dependence on the wavelength of the absorption measured by ATR. The water signal was removed by subtraction of pure water spectrum. Analysis of the conformations of the peptides was performed by deconvolution of the absorption spectra as a sum of Gaussian components with PeakFit 4.12 (Seasolve Software Inc.).

### Fourier Transform Raman Spectroscopy

Fourier transform Raman spectroscopy was performed on the same capillaries as used for SAXS characterization. The spectra were recorded at  $4\text{-cm}^{-1}$  resolution using a Bruker IFS66 interferometer coupled to a Bruker FRA106 Raman module equipped with a continuous Nd:Yag laser providing excitation at 1064 nm.

### Acknowledgements

This work was supported by the biotechnology programme of the French Agency for Research (ANR) with the SmartPep project. F. G. and N. F. were funded by Commissariat à l'Énergie Atomique et aux Énergies Alternatives and CNRS. C. T. was funded by the Région Bretagne through a PhD fellowship. Synchrotron SOLEIL (France) is acknowledged for beam time allocation. The 'TEM-team' platform (iBITec-S/SB2SM) is also acknowledged.

### References

- Chiti F, Dobson CM. Protein misfolding, functional amyloid, and human disease. *Annu. Rev. Biochem.* 2006; **75**: 333–366.
- Kodali R, Wetzler R. Polymorphism in the intermediates and products of amyloid assembly. *Curr. Opin. Struct. Biol.* 2007; **17**(1): 48–57. DOI: 10.1016/j.sbi.2007.01.007.
- Pedersen JS, Andersen CB, Otzen DE. Amyloid structure - one but not the same: the many levels of fibrillar polymorphism: the structural ambiguity of glucagon amyloids. *FEBS J.* 2010; **277**(22): 4591–4601. DOI: 10.1111/j.1742-4658.2010.07888.x.
- Volpatti LR, Vendruscolo M, Dobson CM, Knowles TPJ. A clear view of polymorphism, twist, and chirality in amyloid fibril formation. *ACS Nano* 2013; **7**(12): 10443–10448. DOI: 10.1021/nn406121w.
- Usov I, Adamcik J, Mezzenga R. Polymorphism complexity and handedness inversion in serum albumin amyloid fibrils. *ACS Nano* 2013; **7**(12): 10465–10474. DOI: 10.1021/nn404886k.
- Orgel JP, Irving TC, Miller A, Wess TJ. Microfibrillar structure of type I collagen in situ. *Proc. Natl. Acad. Sci.* 2006; **103**(24): 9001–9005.
- Oda T, Iwasa M, Aihara T, Maéda Y, Narita A. The nature of the globular-to fibrous-actin transition. *Nature* 2009; **461**(7263): 550–550. DOI: 10.1038/nature08440.
- Nogales E, Wolf SG, Downing KH. Structure of the  $\alpha\beta$  tubulin dimer by electron crystallography. *Nature* 1998; **391**(6663): 199–203.
- Nogales E, Whittaker M, Milligan RA, Downing KH. High-resolution model of the microtubule. *Cell* 1999; **96**(1): 79–88.
- Strelkov SV, Herrmann H, Geisler N, Lustig A, Ivaninskii S, Zimbelmann R, Burkhard P, Aebi U. Divide-and-conquer crystallographic approach towards an atomic structure of intermediate filaments. *J. Mol. Biol.* 2001; **306**(4): 773–781. DOI: 10.1006/jmbi.2001.4442.
- Herrmann H, Aebi U. Intermediate filaments: molecular structure, assembly mechanism, and integration into functionally distinct intracellular scaffolds. *Annu. Rev. Biochem.* 2004; **73**(1): 749–789. DOI: 10.1146/annurev.biochem.73.011303.073823.
- Chernyatina AA, Nicolet S, Aebi U, Herrmann H, Strelkov SV. Atomic structure of the vimentin central  $\alpha$ -helical domain and its implications for intermediate filament assembly. *Proc. Natl. Acad. Sci.* 2012; **109**(34): 13620–13625.
- Van Raaij MJ, Mitraki A, Lavigne G, Cusack S. A triple beta-spiral in the adenovirus fibre shaft reveals a new structural motif for a fibrous protein. *Nature* 1999; **401**(6756): 935–938.
- Rossmann MG. Structure of viruses: a short history. *Q. Rev. Biophys.* 2013; **46**(02): 133–180. DOI: 10.1017/S0033583513000012.
- Klug A. From macromolecules to biological assemblies (nobel lecture). *Angew. Chem. Int. Ed. Engl.* 1983; **22**(8): 565–582.
- Luque A, Reguera D. The structure of elongated viral capsids. *Biophys. J.* 2010; **98**(12): 2993–3003. DOI: 10.1016/j.bpj.2010.02.051.
- Luque A, Zandi R, Reguera D. Optimal architectures of elongated viruses. *Proc. Natl. Acad. Sci.* 2010; **107**(12): 5323–5328. DOI: 10.1073/pnas.0915122107.
- Makin OS, Atkins E, Sikorski P, Johansson J, Serpell LC. Molecular basis for amyloid fibril formation and stability. *Proc. Natl. Acad. Sci. U. S. A.* 2005; **102**(2): 315–320.
- Nelson R, Sawaya MR, Balbirnie M, Madsen AØ, Riekel C, Grothe R, Eisenberg D. Structure of the cross- $\beta$  spine of amyloid-like fibrils. *Nature* 2005; **435**(7043): 773–778. DOI: 10.1038/nature03680.
- Sawaya MR, Sambashivan S, Nelson R, Ivanova MI, Sievers SA, Apostol MI, Thompson MJ, Balbirnie M, Wiltzius JJW, McFarlane HT, Madsen AØ, Riekel C, Eisenberg D. Atomic structures of amyloid cross- $\beta$  spines reveal varied steric zippers. *Nature* 2007; **447**(7143): 453–457. DOI: 10.1038/nature05695.
- Ivanova MI, Sievers SA, Sawaya MR, Wall JS, Eisenberg D. Molecular basis for insulin fibril assembly. *Proc. Natl. Acad. Sci.* 2009; **106**(45): 18990–18995.
- Colletier J-P, Laganowsky A, Landau M, Zhao M, Soriaga AB, Goldschmidt L, Flot D, Cascio D, Sawaya MR, Eisenberg D. Molecular basis for amyloid- $\beta$  polymorphism. *Proc. Natl. Acad. Sci.* 2011; **108**(41): 16938–16943.
- Laganowsky A, Liu C, Sawaya MR, Whitelegge JP, Park J, Zhao M, Pensalfini A, Soriaga AB, Landau M, Teng PK, Cascio D, Glabe C, Eisenberg D. Atomic view of a toxic amyloid small oligomer. *Science* 2012; **335**(6073): 1228–1231. DOI: 10.1126/science.1213151.
- Makabe K, McElheny D, Tereshko V, Hilyard A, Gawiak G, Yan S, Koide A, Koide S. Atomic structures of peptide self-assembly mimics. *Proc. Natl. Acad. Sci. U. S. A.* 2006; **103**(47): 17753–17758.
- Fitzpatrick AWP, Debelouchina GT, Bayro MJ, Clare DK, Caporini MA, Bajaj VS, Jaroniec CP, Wang L, Ladizhansky V, Muller SA, MacPhee CE, Waudby CA, Mott HR, De Simone A, Knowles TPJ, Saibil HR, Vendruscolo M, Orlova EV, Griffin RG, Dobson CM. Atomic structure and hierarchical assembly of a cross-amyloid fibril. *Proc. Natl. Acad. Sci.* 2013; **110**(14): 5468–5473. DOI: 10.1073/pnas.1219476110.
- Valéry C, Paternostre M, Robert B, Gulik-Krzywicki T, Narayanan T, Dedieu J-C, Keller G, Torres M-L, Cherif-Cheikh R, Calvo P. Biomimetic organization: octapeptide self-assembly into nanotubes of viral capsid-like dimension. *Proc. Natl. Acad. Sci.* 2003; **100**(18): 10258–10262.
- Valéry C, Artzner F, Robert B, Gulik T, Grabielle-Madellmont C, Torres M-L, Cherif-Cheikh R, Paternostre M. Self-association of a peptide in solution: from  $\beta$ -sheet filaments to large embedded nanotubes. *Biophys. J.* 2004; **86**: 2484–2501.
- Pouget E, Fay N, Dujardin E, Jamin N, Berthault P, Perrin L, Pandit A, Rose T, Valéry C, Thomas D, Paternostre M, Artzner F. Elucidation of the self-assembly pathway of lanreotide octapeptide into  $\beta$ -sheet nanotubes: role of two stable intermediates. *J. Am. Chem. Soc.* 2010; **132**(12): 4230–4241. DOI: 10.1021/ja9088023.
- Valéry C, Pouget E, Pandit A, Verbavatz J-M, Bordes L, Boisdé I, Cherif-Cheikh R, Artzner F, Paternostre M. Molecular origin of the self-assembly of lanreotide into nanotubes: a mutational approach. *Biophys. J.* 2008; **94**(5): 1782–1795. DOI: 10.1529/biophysj.107.108175.
- Pandit A, Fay N, Bordes L, Valéry C, Cherif-Cheikh R, Robert B, Artzner F, Paternostre M. Self-assembly of the octapeptide lanreotide and lanreotide-based derivatives: the role of the aromatic residues. *J. Pept. Sci.* 2008; **14**(1): 66–75. DOI: 10.1002/psc.913.
- Tarabout C, Roux S, Gobeaux F, Fay N, Pouget E, Meriadec C, Ligeti M, Thomas D, IJsselstijn M, Besselièvre F, Buisson D-A, Verbavatz J-M, Petitjean M, Valéry C, Perrin L, Rousseau B, Artzner F, Paternostre M, Cintrat J-C. Control of peptide nanotube diameter by chemical modifications of an aromatic residue involved in a single close contact. *Proc. Natl. Acad. Sci.* 2011; **108**(19): 7679–7684.
- Maurer E, Belloni L, Zemb T, Carrière D. Ion exchange in catanionic mixtures: from ion pair amphiphiles to surfactant mixtures. *Langmuir* 2007; **23**(12): 6554–6560. DOI: 10.1021/la070184w.
- Oda R, Huc I, Schmutz M, Candau SJ, MacKintosh FC. Tuning bilayer twist using chiral counterions. *Nature* 1999; **399**: 566–569.

- 34 Manet S, Karpichev Y, Bassani D, Kiagus-Ahmad R, Oda R. Counteranion effect on micellization of cationic gemini surfactants 14-2-14: Hofmeister and other counterions. *Langmuir* 2010; **26**(13): 10645–10656. DOI: 10.1021/la1008768.
- 35 Oda R, Artzner F, Laguerre M, Huc I. Molecular structure of self-assembled chiral nanoribbons and nanotubules revealed in the hydrated state. *J. Am. Chem. Soc.* 2008; **130**(44): 14705–14712. DOI: 10.1021/ja8048964.
- 36 Stendahl JC, Rao MS, Guler MO, Stupp SI. Intermolecular forces in the self-assembly of peptide amphiphile nanofibers. *Adv. Funct. Mater.* 2006; **16**(4): 499–508. DOI: 10.1002/adfm.200500161.
- 37 Gobeaux F, Fay N, Tarabout C, Mériadec C, Meneau F, Ligeti M, Buisson D-A, Cintrat J-C, Nguyen KMH, Perrin L, Valéry C, Artzner F, Paternostre M. Structural role of counterions adsorbed on self-assembled peptide nanotubes. *J. Am. Chem. Soc.* 2012; **134**(1): 723–733. DOI: 10.1021/ja210299g.
- 38 Gobeaux F, Fay N, Tarabout C, Meneau F, Mériadec C, Delvaux C, Cintrat J-C, Valéry C, Artzner F, Paternostre M. Experimental observation of double-walled peptide nanotubes and monodispersity modeling of the number of walls. *Langmuir* 2013; **29**(8): 2739–2745. DOI: 10.1021/la304862f.
- 39 Oster G, Riley DP. Scattering from cylindrically symmetric systems. *Acta Crystallogr.* 1952; **5**(2): 272–276.
- 40 Harada I, Takeuchi H. Raman and ultraviolet resonance raman spectra of proteins and related compounds. In *Spectroscopy of Biological Systems*. Clark R. J. H., Hester R. E. (eds.). John Wiley & Sons Ltd: New York, 1986; 113–175.
- 41 Tuma R. Raman spectroscopy of proteins: from peptides to large assemblies. *J. Raman Spectrosc.* 2005; **36**(4): 307–319. DOI: 10.1002/jrs.1323.
- 42 Tu AT. Use of Raman spectroscopy in biological compounds. *J. Chin. Chem. Soc.* 2003; **50**(1): 1–10.
- 43 Riekel C, Burghammer M, Schertler G. Protein crystallography microdiffraction. *Curr. Opin. Struct. Biol.* 2005; **15**(5): 556–562. DOI: 10.1016/j.sbi.2005.08.013.
- 44 Roux S, Zékri E, Rousseau B, Paternostre M, Cintrat J-C, Fay N. Elimination and exchange of trifluoroacetate counter-ion from cationic peptides: a critical evaluation of different approaches. *J. Pept. Sci.* 2008; **14**(3): 354–359. DOI: 10.1002/psc.951.
- 45 Le Bail A. Monte Carlo indexing with McMaille. *Powder Diffr.* 2004; **19**(03): 249–254. DOI: 10.1154/1.1763152.

## Supporting Information

Additional supporting information may be found in the online version of this article at the publisher's web site.